Electronic Supplementary Information

Split resonances for simultaneous detection and control measurements in a single Bulk Acoustic Wave (BAW) sensor

Ewelina Wajs,*[a] Girish Rughooobur[b] and Andrew J. Flewitt[a]

[a] Electrical Engineering, University of Cambridge, 9 JJ Thomson Avenue, Cambridge, CB3 0FA, UK.
[b] Microsystems Technology Laboratories, Massachusetts Institute of Technology, 60 Vassar Street, Cambridge, MA02139, USA.

Corresponding Author:* *emw62@cam.ac.uk*

Experimental Section

1. Fabrication and characterization of solidly mounted resonators

The SMR fabrication process begins with the sputter deposition of 5 layers of acoustic reflectors alternating between SiO_2 and Mo on 100 mm diameter 100 oriented *n*-type 500 µm thick Si wafers. A layer of Ti (20 nm) as adhesion layer and the bottom electrode Ir (120 nm) are sequentially evaporated by electron beam evaporation. Note the bottom electrode is not patterned and instead left as a floating ground. The piezoelectric layer of ZnO is deposited in a High Target Utilization Sputtering (HiTUS, S500, PlasmaQuest Ltd., Hooke, UK) system at a pressure of 2.2×10^{-3} mbar with 30 sccm of Ar and 37 sccm of O_2 using a 99.999% purity and 100 mm diameter Zn target (Testbourne Ltd, Basingstoke, Hampshire, UK). A launch RF (13.56 MHz, MKS RF Generator, Andover, MA, USA) power of 1200 W and a DC target power of 1000 W are used. The substrate is located at a distance offset by ~30° from the target axis and purposefully not rotated to promote the ZnO grains to grow in off-axis orientation to obtain quasi-shear modes as explained in our previous works.[17,21] A cross-sectional scanning electron microscope (SEM, Carl-Zeiss Sigma VP, Oberkochen, Germany) image of the inclined ZnO grains is shown in Figure S1. After 0.85 µm thick ZnO deposition, the top electrode of Mo (~120 nm thick) is deposited by magnetron sputtering system (WhiteMagic, Precision Atomics Ltd, Cambridge, UK) at a pressure of 3.5×10^{-3} mbar, 30 sccm of Ar, deposition power of 100 W using a 100 mm diameter 99.95% purity Mo target (Pi-KEM, Wilnecote, Tamworth, UK). Using an EV620 (EVG, St Florian Am Inn, Austria) photolithography system the top electrode is patterned using Microposit S1818 photoresist and developed using MF319 developer. A CF_4/O_2 reactive ion etch with 100 W RF power, 150 mTorr pressure, and 25% O_2 in CF_4 is used to define the top electrode. The photoresist is then removed from the surface of the device by sequential sonication in solutions of acetone, iso-propanol and de-ionized water. The pentagonal region for the functional layer is patterned by standard ultra-violet photolithography using AZ2020 nLoF photoresist. By means of thermal evaporation (E306, Edwards, West Sussex, UK), both 5 nm of Cr is deposited as an adhesion layer for the subsequent Au layer, the thickness of which is varied from 5 to 30 nm. Lift-off of the excess Au and Cr layers is carried out in *n*-methyl-2-pyrrolidone, acetone, iso-propanol and de-ionized water to leave a pentagonal shape region (area of 1.42×10^{-4} cm^2) on the resonator with the added Au/Cr layer.

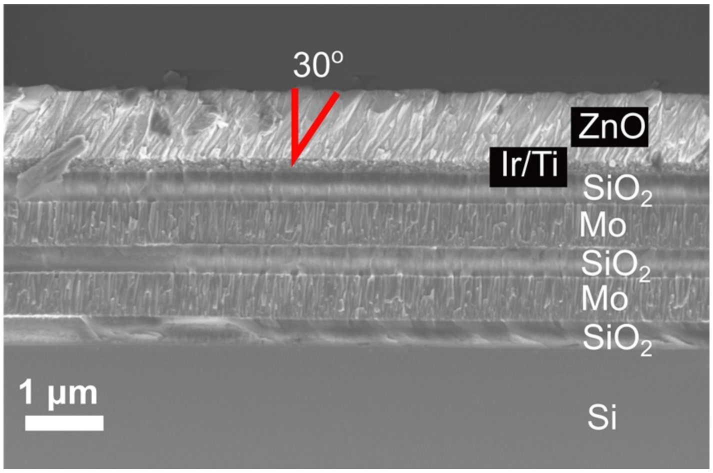

Figure S1: Cross-section of a fabricated stack of thin films without the top Mo electrode observed with SEM demonstrating the thicknesses of the layers, and the tilt of ~30° in the ZnO grains relative to the normal axis orientation, thereby giving rise to a quasi-shear mode (shear and longitudinal).

The surface of the inclined *c*-axis ZnO was mapped using atomic force microscopy (Agilent 5500 scanning probe microscope, Palo Alto, CA, USA) and shown in Figure S2 (a). The extracted profile of the ZnO layer using Gwyddion (http://gwyddion.net/) is shown in Figure S2 (b). A root mean square roughness (rms) value of 14.4 nm was obtained over a 10 µm scan region, which quantifies the surface roughness of the piezoelectric layer; this can lead to acoustic wave scattering and hence a loss mechanism that deteriorates the electromechanical performance.

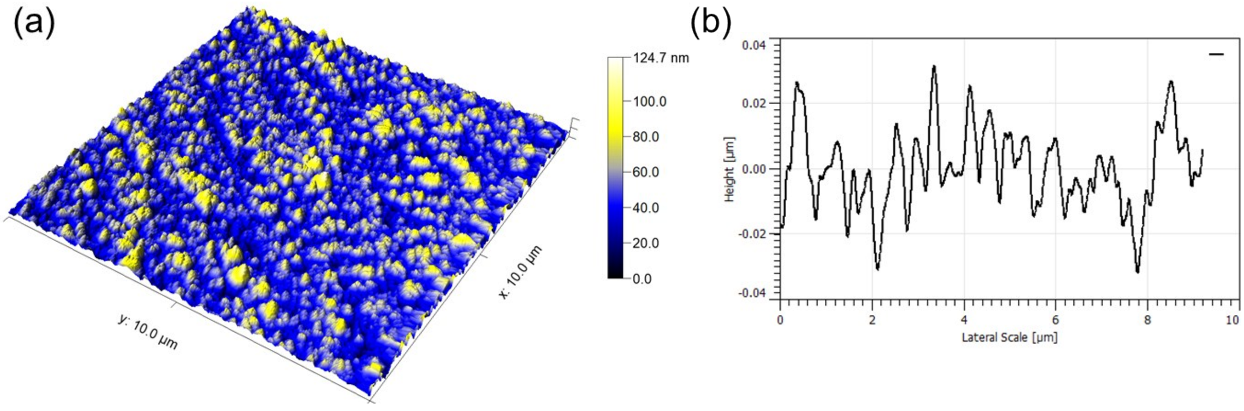

Figure S2: (a) 3D image of the AFM scan of a 10 µm scan of the ZnO layer sputtered on acoustic reflector stack, (b) An extracted profile across the AFM scan to demonstrate the rough profile of the piezoelectric layer.

Measured electrical admittance (magnitude and phase) responses are shown in Figure S3, and the electromechanical coupling coefficients together with the quality-factors (Q_r) at resonance are calculated using equations 1 and 2 respectively for both the thickness shear (TSM) and the longitudinal (TLM) modes and listed in Table S1.

$$Q_r = \frac{f_r}{2} \left| \frac{\mathrm{d}\Phi_Y}{\mathrm{d}f} \right|_{f\,=\,f_r} \quad (1)$$

$$k_{eff}^2 = \frac{\pi f_s}{2 f_p} \frac{1}{\tan\left(\frac{\pi f_s}{2 f_p}\right)} \quad (2)$$

where f_r is the resonance frequency, Φ_Y is the phase of the electrical admittance, f_s is the series frequency of the resonance (can be approximated to the resonant frequency where electrical impedance (Z) is zero/minimum), and f_p is the parallel frequency of the resonance (can be approximated to the anti-resonance frequency, f_a, where electrical admittance (Y) is zero/minimum).

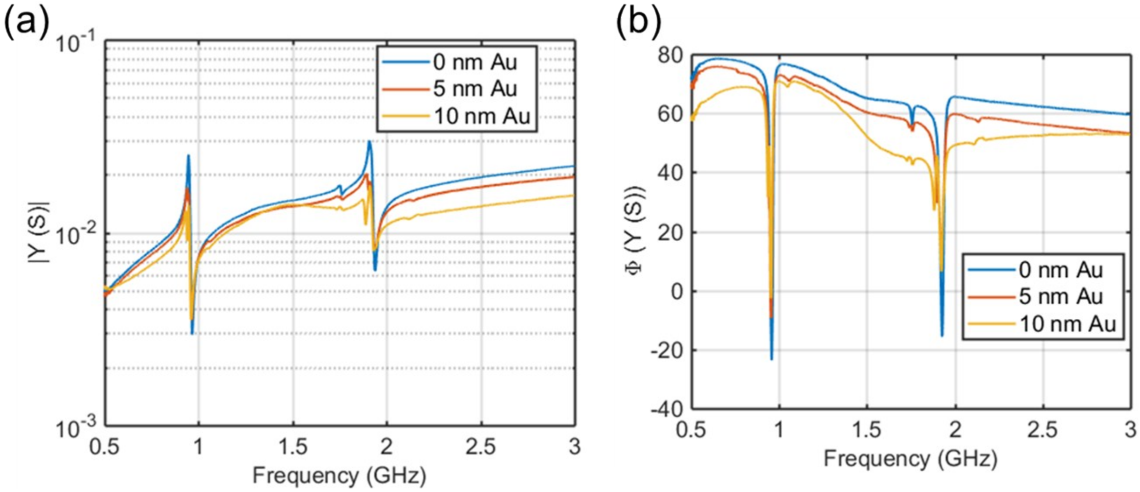

Figure S3: (a) Magnitude of the electrical admittance spectra for no Au, 5 nm and 10 nm Au on R1 of the SMR devices used to calculate the electromechanical coupling coefficients. (b) Phase of the electrical admittance spectra for no Au, 5nm and 10 nm of Au on the SMR devices used to calculate the Q-factors.

Table S1: Measured Q-factors and electromechanical coupling coefficients of each resonance.

0 nm Au	f_r (GHz)	f_a (GHz)	Q_r	k_{eff}^2 (%)
TSM f_2	0.948	0.965	65	4.27
TLM f_2	1.914	1.937	61	2.90
5 nm Au	f_r (GHz)	f_a (GHz)	Q_r	k_{eff}^2 (%)
TSM f_1	0.942	0.945	37	0.91
TSM f_2	0.949	0.960	66	3.05
TLM f_1	1.897	1.904	24	0.90
TLM f_2	1.914	1.930	39	2.03
10 nm Au	f_r (GHz)	f_a (GHz)	Q_r	k_{eff}^2 (%)
TSM f_1	0.934	0.938	34	0.84
TSM f_2	0.949	0.960	70	2.92
TLM f_1	1.878	1.889	18	1.30
TLM f_2	1.913	1.930	49	2.28

2. Simulation parameters of each layer in the SMRs

The linear elastic materials in the structure were simulated using the default COMSOL® Multiphysics 5.3 Library properties shown in Table S2, using the thicknesses obtained experimentally from the SEM cross-section shown in Figure S1.

Table S2: Material properties of the electrodes and reflector materials used in the FEM simulations.

Material	Density (kg/m^3)	Young's Modulus (GPa)	Poisson Ratio	Thickness (nm)
Mo	10200	312	0.30	120 (Electrode), 647 (Reflector)
Ti	4506	115.7	0.32	20
Au	19300	70	0.44	0-30
Ir	22900	528	0.26	120
Cr	7150	279	0.21	5
SiO_2	2200	70	0.17	585

The Si substrate was simulated as an anisotropic linear material as it is a single crystal. The thickness used in the simulation was 10 µm but with a perfectly matched layer at the bottom to produce the effect of a 500 µm thick Si wafer. The elastic parameters for the anisotropic Si crystal are given as follows:

Density = 2330 kg/m^3

Elasticity matrix, $$c = \begin{pmatrix} 166 & 64 & 64 & 0 & 0 & 0 \\ 0 & 166 & 64 & 0 & 0 & 0 \\ 0 & 0 & 166 & 0 & 0 & 0 \\ 0 & 0 & 0 & 80 & 0 & 0 \\ 0 & 0 & 0 & 0 & 80 & 0 \\ 0 & 0 & 0 & 0 & 0 & 80 \end{pmatrix} \text{ GPa}$$

The ZnO piezoelectric crystal was simulated using the following stress-charge form with a rotated piezoelectric model. The thickness used was 0.85 µm in the simulation.

Density = 5680 kg/m^3

Elasticity matrix, $$c = \begin{pmatrix} 209.7 & 121.1 & 105.3 & 0 & 0 & 0 \\ 0 & 209.7 & 105.3 & 0 & 0 & 0 \\ 0 & 0 & 211.1 & 0 & 0 & 0 \\ 0 & 0 & 0 & 42.4 & 0 & 0 \\ 0 & 0 & 0 & 0 & 42.4 & 0 \\ 0 & 0 & 0 & 0 & 0 & 44.2 \end{pmatrix} \text{ Gpa}$$

Coupling matrix, $$e = \begin{pmatrix} 0 & 0 & 0 & 0 & -0.48 & 0 \\ 0 & 0 & 0 & -0.48 & 42.4 & 0 \\ -0.56 & -0.56 & 1.32 & 0 & 0 & 44.2 \end{pmatrix} \text{ C/m}^2$$

Relative permittivity, $$\varepsilon = \begin{pmatrix} 8.55 & 0 & 0 \\ 0 & 8.55 & 0 \\ 0 & 0 & 10.2 \end{pmatrix}$$

The ZnO layer is also simulated with a rotated crystal with the rotation angle of the *z*-axis to be $\beta = 30°$ as shown in Figure S4, whereas all other films in the stack were kept to be on the same global coordinates with no rotation.

Perfectly matched layers (10 µm wide) were added on all the sides and on all layers (except the top electrode and Au/Cr layer) of the structure in the simulation to prevent unwanted edge reflections and hence model the effects of a continuous and wide film similar to the real device.

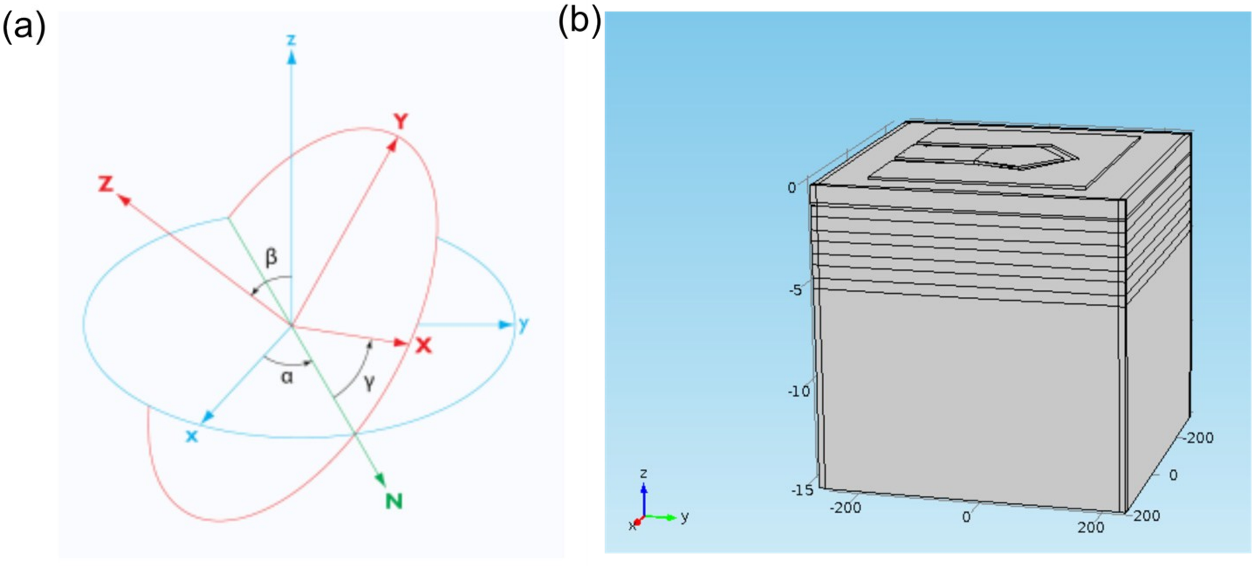

Figure S4: (a) The coordinate system of the piezoelectric layer in COMSOL® Multiphysics 5.3 and the related angles to change the crystal orientation; (b) The axis orientation relative to the device used in the simulation.

The simulation setup was divided across the top electrode due to symmetry and a boundary condition was applied to half the structure, which eventually helps in reducing the computation time to approximately 6 hours on a 2.0 GHz Intel i7 CPU and 16 GB RAM computer.

For a more realistic simulation, a low reflecting boundary condition and mass damping were used at the ZnO and the top electrode interface to account for the roughness of the ZnO layer (as shown in Figure S2) and mass added by increased Au thickness respectively. Using finite element method, the phase was simulated and the quality-factors of Au thickness (0-30 nm) on R1 of the SMR were calculated using equation 1 shown in section 1 of this Supporting Information. These are displayed in Figure S5 and S6 respectively. In Figure S6 (a) and Figure S6 (b), the quality-factors at resonance are the values in the negative quadrant whereas at anti-resonance the *Q*-factors are in the positive quadrants. It is therefore shown that the devices have quality factors < 200, without accounting all the roughness and material property differences of each layer. As the thickness of Au increases, the *Q*-factors for both the TSM and TLM decrease to lower than 100.

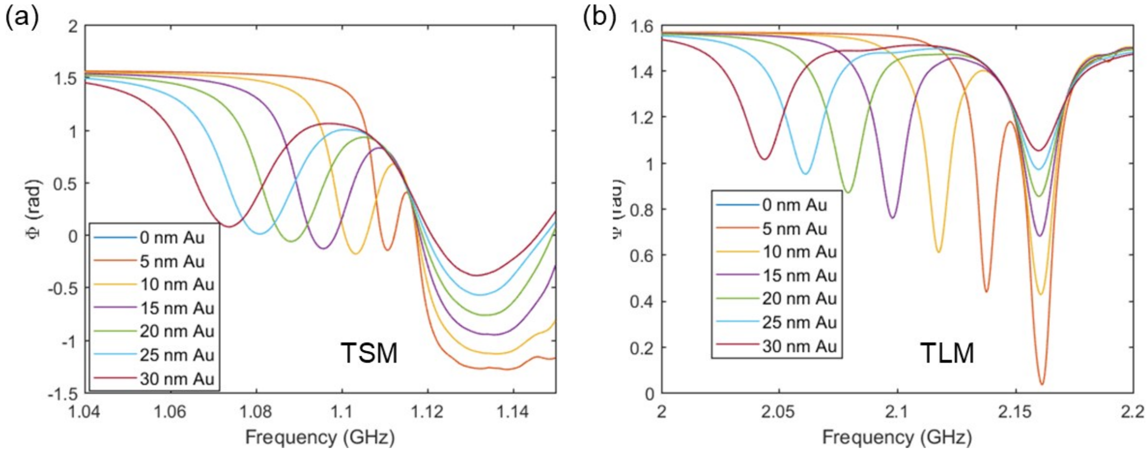

Figure S5: (a) The phase in radians of all the Au thicknesses of the thickness shear mode obtained from finite element method analysis of the SMR structure; (b) Corresponding phase in radians for the thickness longitudinal mode obtained from the finite element modelling.

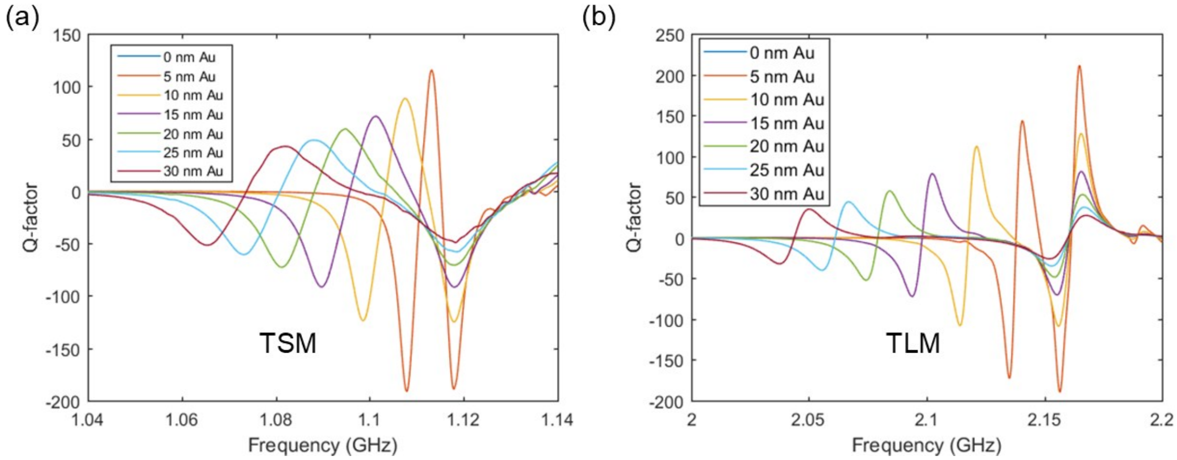

Figure S6: (a) Derived Q-factors of all the Au thicknesses for the thickness shear mode obtained from finite element method analysis (b) Corresponding derived Q-factors for the thickness longitudinal mode obtained from finite element method simulation.

To obtain exact frequency positions, quality-factors and electromechanical couplings is beyond the scope of this work as the properties of each layer will have to be characterized individually and each layer will have to be grown on its corresponding layer according to the SMR structure. Here the frequency shifts that are used as a mass sensing mechanism are the most important factor rather than the absolute positions or the electromechanical coupling the resonances.

4. Temperature variations experiment

Figure S7 displays the results of tracking the difference between the two frequencies (f_2 - f_1) in TLM as function of temperature. For this experiment a clean device chip (25 devices) was used with the Au thickness of approximately 20 nm, which was gradually heated up to 48 °C using a probe station with incorporated heating unit. The changes in the frequency were recorded for each temperature point ranging from 22 °C to 48 °C.

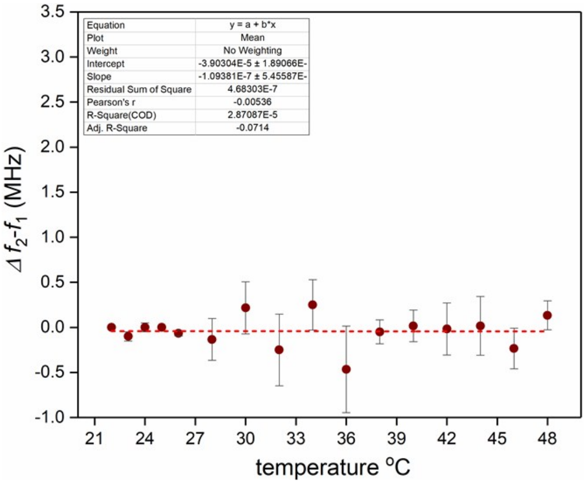

Equation	y = a + b*x
Plot	Mean
Weight	No Weighting
Intercept	-3.90304E-5 ± 1.89066E-
Slope	-1.09381E-7 ± 5.45587E-
Residual Sum of Square	4.68303E-7
Pearson's r	-0.00536
R-Square(COD)	2.87087E-5
Adj. R-Square	-0.0714

Figure S7: Difference between the resonant frequencies f_2 - f_1 for the TLM changing with the temperature (°C) increase.

As it can be seen in Figure S7 the largest frequency shift variations can be observed with higher temperatures (~30 °C – 48 °C), however at room temperatures (~22 °C – 30 °C) these variations are negligible and will have very little impact in a temperature controlled environment such as an air-conditioned room where variations are only ~±1 °C, what can further result in a very accurate mass sensing tool.

5. Surface sensing experiment

Materials: 11-mercaptoundecanoic acid 98% from Sigma-Aldrich was used as received without any further purification, fabricated SMR devices with approx. ~20 nm of Au were used in this experiment.

SMR devices were fabricated as described in section 1 and clean Au surface of the device was exposed to the thiol molecules by immersing the device in the ethanolic solution of 11-mercaptoundecanoic acid at different concentrations (0 mM, 0.02 mM, 0.15 mM, 1.25 mM, 5 mM, 50 mM, 100 mM) for a minimum of 3 hours at 4 °C. At the end of the incubation time each device was thoroughly rinsed with pure ethanol to remove excess of the unattached thiol molecules and dried with N_2.

The sensor response to the attachment of the thiol molecules (11-MUA) to the Au surface was monitored by measuring the real part of the electrical admittance (Y) in the frequency range from 0.5 GHz to 3.0 GHz and it is shown in the Figure S8.

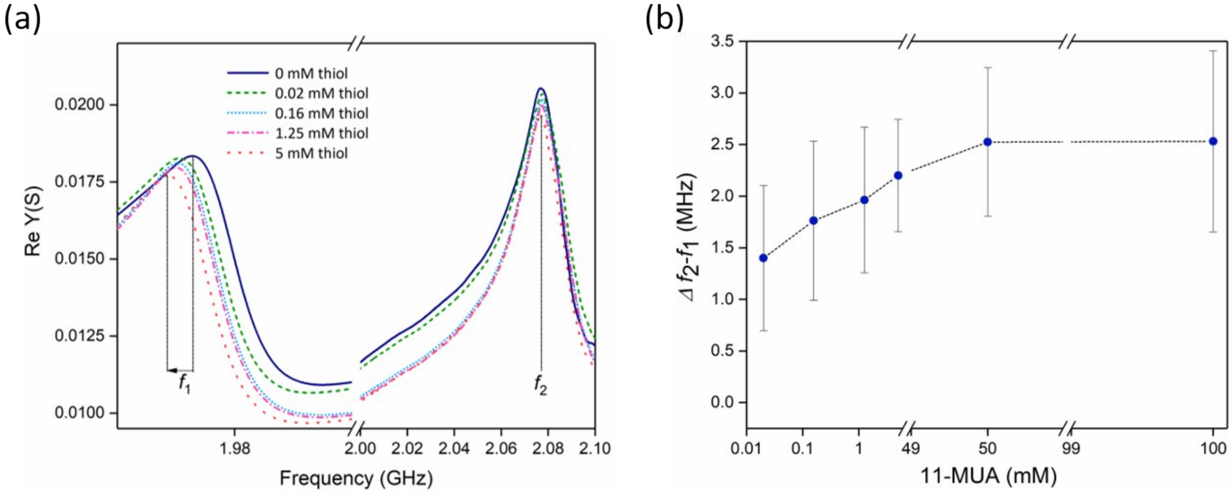

Figure S8: The increase in the difference between the two resonances f_2 - f_1 observed in TLM of SMR device due to attachment of thiol molecules onto Au surface in SMR device. (a) TLM showing split modes, where the mass sensitive mode (f_1) shifts towards lower frequencies due to the attachment of thiol molecules to the Au surface. (b) Observed increase in the difference between the resonant frequencies f_2 - f_1 for the TLM with higher concentrations of the thiol molecules for ~20 nm Au; (the dashed line is here for better visibility).

From these experiments we can conclude that the tracking of the attachment of thiol molecules to the Au surface of SMR device is possible by simply calculating the increase in the distance of the two resonant frequencies (f_2 - f_1); this increase is observed as the mass sensitive frequency (f_1) shifts towards lower frequencies because of more molecules being attached to the Au surface of the SMR device (as shown in Figure S8 (a)). Additionally, as can be seen in the Figure S8 (b) the standard deviation from 5 measurements for each thiol concentration is quite high, however we present here the initial findings from sensing experiments as a proof of concept and optimization of an assay for sensing different analytes is currently ongoing in our research group.